SPHERICAL DIFFUSION FLAME IN MICROGRAVITY CONDITIONS: FIRST RESULTS OF JOINT RUSSIAN–AMERICAN SPACE EXPERIMENT FLAME DESIGN — ADAMANT

S. M. Frolov

N. N. Semenov Federal Research Center for Chemical Physics
of the Russian Academy of Sciences
4 Kosygin Str., Moscow 119991, Russian Federation
e-mail: smfrol@chph.ras.ru

The joint NASA – Roscosmos Flame Design (Adamant) spaceflight experiment is one of six International Space Station (ISS) investigations which are currently a part of the Advanced Combustion via Microgravity Experiments (ACME) project. The objective of the spaceflight experiment is to study normal and inverse (with respect to the direction of forced convection) spherical diffusion ethylene–oxygen diluted flames around a porous sphere (PS) in microgravity when the flame structure can be isolated from natural convection effects. The experiment is focused on revealing the conditions of flame extinction caused by radiative heat loss and the onset (inception) of soot. The data from the experiment are used for validating numerical simulations based on the physical and mathematical models of different complexity including detailed/reduced chemical mechanisms of fuel oxidation, species transport, and radiative heat transfer. It is expected that the project will improve our understanding of flame physics and chemistry and provide novel solutions for controlled combustion with reduced pollutants in terrestrial applications. The paper presents some experimental and computational results obtained so far by the international research team.

1 Introduction

In terrestrial conditions, gravity can have a strong effect on the combustion process, especially if the flame propagates at low speeds. High-temperature combustion products, having a significantly lower density than the initial gas, under the action of the buoyancy (Archimedes) force acquire a directed upward movement. At zero gravity, the buoyancy force is absent. The arising difference can be illustrated by the example of burning a droplet of liquid motor fuel at rest which is accompanied by the formation of microscopic soot particles.

DOI: 10.30826/NEPCAP9B-13

Soot is formed in the region between the droplet and the flame due to thermal decomposition of fuel vapors in the presence of high-temperature combustion products. Under terrestrial conditions, the formed soot particles, together with the combustion products, are gradually carried upward from the drop due to the buoyancy force, and new particles are formed in the region between the drop and the flame. This happens until the drop completely burns out. If gravity is "turned off" (zero gravity conditions), the carryover of soot particles will stop: the particles will accumulate in the region between the drop and the flame, forming a loose spherical soot "shell." Such a shell becomes a kind of screen for the heat flux directed from the flame to the drop. The droplet evaporation slows down, the flame is extinguished, and the droplet remains unburned. Under certain conditions (after the dispersion of the soot shell), repeated spontaneous ignition and extinguishing of the droplet may occur. Thus, there are fundamental differences in the behavior of a drop in terrestrial conditions and in zero gravity. This means that the development of a fire during the spills of flammable liquids under terrestrial conditions and under zero gravity conditions, for example, on a manned spacecraft, can be completely different. In view of the importance of this issue, at the ISS, since 2017, Russian–American space experiments (SE) have been carried out to study the specific features of combustion of gases, liquids, and solid materials in zero gravity [1, 2]. So, in 2017–2018, SE "CFI–Zarevo" (CFI stands for Cool Flame Investigation) was carried out, in which the phenomenon of extinction of a drop of heavy hydrocarbon fuel was studied [3], and in 2019 — SE "Flame Design — Adamant," in which the study of the phenomenon of extinction of a spherical flame of unmixed gases, the so-called spherical diffusion flame (SDF), began. We will focus further on the SE "Flame Design — Adamant."

The objective of the SE "Flame Design — Adamant" is the experimental and theoretical study of the fundamental mechanisms of controlling soot formation in the SDFs observed under zero gravity conditions.

2 Space Experiment

NASA designed and manufactured an experimental setup which was delivered to the ISS. The international crew prepared the unit for operation. The setup includes a combustion chamber (CC), in the central part of which a PS is placed on a straight gas supply tube (Fig. 1*a*), auxiliary devices, and recording equipment (video cameras, radiometers, photomultipliers, and thermocouples). The setup operates in automatic mode. At the beginning of the experiment, the CC is filled with gas, for example, air. Then, a gaseous fuel — a mixture of ethylene and nitrogen or pure ethylene — is fed into the PS with a mass flow rate of several milligrams per second, and the ignition is switched on at the same time. With a successful ignition, an SDF is formed around the PS. The entire com-

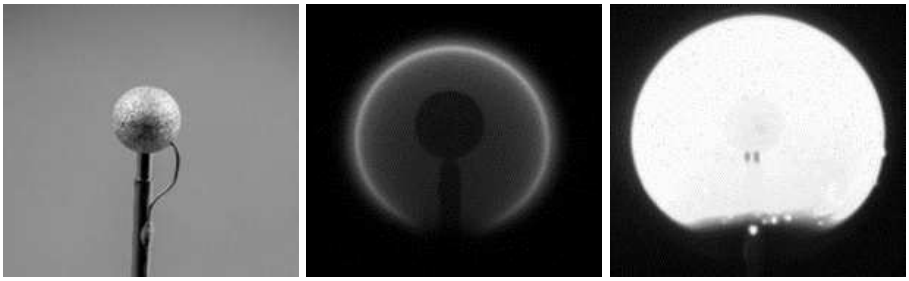

(*a*) (*b*) (*c*)

Figure 1 A PS with a thermocouple and a gas supply tube (*a*); nonsooting diffusion flame (*b*); and sooting diffusion flame (*c*)

bustion process (lasting up to about 200 s) is recorded by digital video cameras. Frame-by-frame analysis of flame images allows one to obtain the dependence of the flame radius on time. During the experiment, the temperature of the PS, measured by the thermocouple, increases. For the safety of the PS, the experiment is terminated if its temperature exceeds 500 °C. The SDF temperature is determined by the readings of radiometers measuring the radiation intensity of thin (15 μm) heat-resistant silicon carbide fibers placed in a flame. The experiments change the mass flow rate and composition (the degree of dilution with nitrogen) of the gas supplied through the PS, as well as the composition and pressure of the gas atmosphere in the CC. The operation of the equipment is synchronized, and the information received via radio communication channels is sent to the Mission Control Center in real time.

The experiments are planned to investigate "direct" and "inverse" SDFs. The direct flame is the flame formed when a combustible gas is supplied to the PS. In this case, the CC is filled with an oxidizing gas — a mixture of oxygen and nitrogen. This flame simulates the combustion of a drop of liquid fuel. The inverse flame is the flame formed when an oxidizing gas is supplied to the PS, while the CC is initially filled with a combustible gas. Such a flame simulates the combustion of a drop of a liquid oxidizer in fuel vapor.

At the first stage of SE in 2019, 188 experiments with direct ethylene flames were carried out. The crew monitored the implementation of the experiment program, replaced containers with gases and liquids, adjusted the equipment, and, if necessary, replaced faulty components. In the experiments, various physical and chemical phenomena were registered, including the new ones: (*i*) the formation of a stable, nonsooting, blue SDFs (Fig. 1*b*); (*ii*) the formation of a nonsooting SDFs with a sudden spontaneous extinction; (*iii*) the formation of a nonsooting SDFs with the development of radial oscillations of the front and spontaneous extinction; (*iν*) the formation of sooting SDFs of a bright yellow color with a sud-

den spontaneous extinction (Fig. 1*c*); (ν) the formation of sooting SDFs with the development of radial oscillations of the front and spontaneous extinction; (νi) the formation of an asymmetric sooting flame with front oscillations and spontaneous extinction; (νii) the formation of soot superagglomerates penetrating the flame, etc. Experiments have shown that before extinguishing, the flame temperature decreases to 900–1000 °C. The results of some earlier investigations of the SDFs can be found elsewhere [4–9].

3 Numerical Simulation of Spherical Diffusion Flames

Within the project, the Russian research team from the Semenov Federal Research Center for Chemical Physics of the Russian Academy of Sciences investigates the SDF theoretically using numerical simulation. It was implied to develop a predictive physical and mathematical model that reproduces the observed phenomena. With such a model, it is possible to determine the conditions for the radiation extinction of the SDF and to study the influence of various external effects (gasdynamic, acoustic, thermal, and chemical) on soot formation. In addition, based on such a model, it is possible to perform an express analysis of experimental data and issue scientifically grounded recommendations for changing the modes of performing the SE. This section briefly describes the model as well as the results of calculations and their comparison with the experimental data obtained at the first stage of the SE "Flame Design — Adamant."

3.1 Phenomenology

The PS with a radius of $r_s = 3.2$ mm and a permeability κ is made by sintering from stainless steel particles. A gas supply tube with a flow cross-section area S_{in} (inner diameter 1.5 mm) is inserted into the PS to a depth of $r = 2.5$ mm. The volume of the CC, V, in which the assembly is placed is approximately 90 l (the radius of the outer wall $r_\infty = 288$ mm). Initially, at time $t = 0$ s, the entire CC is filled with a nitrogen–oxygen mixture with a temperature T_0, pressure P_0, and species mass fractions Y_{i0} (hereinafter, the index i refers to a specific species in the mixture). At $t > 0$, a combustible gas — a mixture of ethylene and nitrogen — with the preset constant species mass fractions $Y_{i,\text{in}}$ is supplied through the gas supply tube and the PS with a constant mass flow rate G_{in} (hereinafter, the index 'in' refers to the cross section of the combustible gas supply). Combustible gas, passing through the pores of the PS, displaces the initial nitrogen–oxygen mixture from it and enters the CC. The supply of combustible gas through the PS is accompanied by molecular mixing of gases and the formation of a combustible mixture in the vicinity of the PS which is ignited by an external ignition source at time t_{ign}. After a certain transition period, an SDF is formed around the PS and the maximum temperature in the flame is reached at a certain distance r_f from the PS center called the flame

radius. During combustion, the position of the flame can change: the flame radius can increase and/or decrease. Depending on the governing parameters of the problem (G_{in}, $Y_{i,\text{in}}$, Y_{i0}, etc.), situations are possible when $r_f > r_s$ and $r_f \leqslant r_s$. Combustion in the flame is accompanied not only by chemical energy release but also by the processes of radiation and heat removal into the surrounding space. The sources of radiation are mainly triatomic molecules (CO_2 and H_2O) as well as soot which can form during combustion. Heat flux from the flame heats up the gas supply tube, the PS, and the combustible gas flowing through the PS. The latter leads to a change in the density of the combustible gas and, consequently, to an increase in its linear velocity at the outer surface of the PS which can affect the flame radius.

3.2 Statement of the problem

The physical and mathematical model must take the most important processes involved in the described phenomenology into account. Since the Navier–Stokes equations are valid for both nonporous and porous media, for solving the problem, we apply the general three-dimensional (3D) time-dependent Reynolds-averaged Navier–Stokes (RANS), energy, and species conservation equations for a multicomponent reacting mixture:

$$\rho\frac{\partial U_i}{\partial t} + \rho U_j\frac{\partial U_i}{\partial x_j} = -\frac{\partial P}{\partial x_i} + \frac{\partial}{\partial x_j}\left[\tau_{ij} + \tau_{ij}^t\right]; \tag{1}$$

$$\rho\frac{\partial I}{\partial t} + \rho U_j\frac{\partial I}{\partial x_j} = \rho\dot{Q} + \frac{\partial P}{\partial t} + \frac{\partial}{\partial x_j}\left[\left(\tau_{ij} + \tau_{ij}^t\right)U_j\right] + \frac{\partial}{\partial x_j}\left(q_j + q_j^t\right) + \Omega; \tag{2}$$

$$\rho\frac{\partial Y_l}{\partial t} + \rho U_j\frac{\partial Y_l}{\partial x_j} = \rho\dot{w}_l + \frac{\partial}{\partial x_j}\left[\rho\left(j_{lj} + j_{lj}^t\right)\right]. \tag{3}$$

Here, t is the time; x_j $(j = 1, 2, 3)$ is the Cartesian coordinate; ρ is the mean density; P is the mean pressure; U_i is the ith component of the mean velocity vector; τ_{ij} is the tensor of viscous stresses; τ_{ij}^t is the tensor of turbulent (eddy) stresses; $I = H + 0.5\sum_i U_i^2$ is the mean total enthalpy where H is the mean static enthalpy; q_j is the molecular heat flux; q_j^t is the turbulent (eddy) heat flux; Y_l $(l = 1, \ldots, N)$ is the mean mass fraction of the lth species where N is the total number of species in the mixture; $\dot{w}_l$ and $\dot{Q}$ are the mean sources of mass and energy due to chemical transformations; q is the heat flux; Ω is the heat source/sink other than that of chemical nature; and j_{lj} and j_{lj}^t are the molecular and turbulent mass fluxes of the lth species, respectively. The turbulent fluxes of species, momentum, and energy in Eqs. (1) to (3) can be modeled, e. g., within the framework of a certain turbulence model. The governing equations are closed by the caloric and thermal equations of state, the reaction mechanism of fuel oxidation and soot formation, the relationships for the fluxes and source terms as well as by the initial and boundary conditions.

According to the phenomenology, the following simplifying assumptions can be adopted.

1. The gas supply tube does not affect the evolution of the SDF.
2. All physicochemical processes are spherically symmetric, so that the one-dimensional (1D) approximation is valid.
3. The porous medium in the flow region can be modeled by flow resistance according to the Darcy law and heat exchange with the fluid according to the Newton law, i. e., the porous medium can be represented by added momentum and heat sources, $(\partial P/\partial x_i)_s$ and Ψ_s, respectively, in the governing equations. Also, since the porous medium reduces the volume accessible for fluid, the local flow velocity, U_i, and superficial velocity inside the porous medium, u_i, are coupled by the undirected porosity value φ: $U_i = \varphi u_i$.
4. The thermophysical and structural parameters of the PS material are constant.
5. Thermal radiation of PS is negligible; PS absorbs thermal radiation of soot, H_2O, CO_2, N_2, and O_2.
6. Gas-phase and catalytic reactions in the PS are absent.
7. The gas flow is laminar.
8. A multicomponent gas mixture obeys the thermal and caloric equations of state of an ideal gas and possesses variable thermophysical properties.
9. The effect of thermodiffusion is negligible.
10. Soot is an equivalent gas with the molecular mass of atomic carbon.
11. Soot particles have a constant size and do not coagulate.
12. The radiation heat flux is caused solely by soot, H_2O, CO_2, N_2, and O_2 emittance.
13. The outer wall of the computational domain is impermeable, noncatalytic, and isothermal.

Following assumptions 1 and 2, the computational domain can be represented in the form of a central sector with a small opening angle divided into control volumes in the radial direction. Following assumptions 3 to 6, the 1D energy conservation equation for the porous medium reads:

$$\rho_s c_s \frac{\partial T_s}{\partial t} = \lambda_s \frac{\partial}{\partial x_j}\left(\frac{\partial T_s}{\partial x_j}\right) + \Omega_s \tag{4}$$

where ρ_s, c_s, λ_s, and T_s are the density, specific heat, thermal conductivity, and temperature of the PS material; and Ω_s is the heat source/sink for the PS. Moreover, assumptions 3 and 5 mean that the term Ω_s in Eq. (4) contains only two contributions: Ψ_s and the radiation absorption $\Omega_{\rm sg}$, whereas assumption 4 implies that the PS radius r_s is constant. Following assumption 7, the turbulent fluxes in Eqs. (1) to (3) can be omitted, i. e., $\tau_{ij}^t = q_j^t = j_{lj}^t = 0$. Assumption 8 is conventional and implies the validity of the equations of state:

$$p = \rho RT \sum_{l=1}^{N} \frac{Y_l}{m_l}\,; \tag{5}$$

$$H_l = H_l^0 + \int_{T^0}^{T} c_{p,l}\, dT \tag{6}$$

where m is the molecular mass; R is the universal gas constant; T is the temperature; N is the total number of species in the gas; H^0 is the standard enthalpy of formation at temperature T^0; and c_p is the specific heat at constant pressure. Assumption 9 means that molecular fluxes q_j and j_{lj} can be determined as

$$q_j = -\lambda \frac{\partial T}{\partial x_j}\,; \quad j_{lj} = -D_l \frac{\partial Y_l}{\partial x_j}\,, \quad l = 1, \ldots, N-1\,, \tag{7}$$

where λ is the thermal conductivity and D_l is the effective diffusion coefficient of the lth species in the mixture [10]. Assumption 10 means that soot is considered as a gaseous species in the reaction mechanism with its own mass fraction, $Y_{\rm soot}$. However, for estimating the effect of soot radiation, we conditionally assume (assumption 11) that soot particles possess the specific (per unit mass) emitting surface, $S_{\rm soot} = 6/(d_{\rm soot}\rho_{\rm soot})$ (here, $d_{\rm soot}$ is the conditional soot particle size and $\rho_{\rm soot}$ is the soot density) which is directly connected to the soot mass fraction $Y_{\rm soot}$. Assumption 12 implies that the source term Ω in Eq. (2) contains the contribution $\Omega_{\rm soot}$ proportional to $S_{\rm soot}$. Assumption 13 implies that the term Ω in Eq. (2) contains the contribution Ω_g proportional to the local instantaneous volume fractions of H_2O, CO_2, N_2, and O_2. Assumption 13 is conventional.

Thus, the 3D governing equations (1) to (4) are greatly simplified and can be solved in 1D approximation using an available computational fluid dynamics (CFD) code. The explicit form of the source terms entering Eqs. (1) to (4) are as follows:

$$\dot{w}_l = m_l \sum_{k=1}^{L} \left(\nu''_{l,k} - \nu'_{l,k}\right) A_k T^{n_k} \exp\left(-\frac{E_k}{RT}\right) \prod_{j=1}^{N} \left(\frac{Y_j \rho}{m_j}\right)^{\nu'_{l,k}}\,; \tag{8}$$

$$\dot{Q} = \sum_{l=1}^{N} H_l \dot{w}_l\,; \tag{9}$$

$$\Omega = \Omega_{\text{soot}} + \Omega_g + \Psi_s \,; \tag{10}$$

$$\Omega_{\text{soot}} = \sigma S_{\text{soot}} Y_{\text{soot}} \rho \left(T^4 - T_0^4\right) \,; \tag{11}$$

$$\Omega_g = \sigma P \sum_{l=1}^{4} a_l(T) X_l \left(T^4 - T_0^4\right) \,; \tag{12}$$

$$\Psi_s = \alpha_s S_{\text{PS}} (T - T_s) \,; \tag{13}$$

$$\Omega_s = \Psi_s + \Omega_{\text{sg}} \,; \tag{14}$$

$$\Omega_{\text{sg}} = \delta_s \varepsilon_s \int (\Omega_{\text{soot}} + \Omega_g)\, dV \,; \tag{15}$$

$$\left(\frac{\partial P}{\partial x_i}\right)_s = \left(\frac{\partial P}{\partial x}\right)_s = \frac{\mu}{\kappa}\, u \tag{16}$$

where L is the total number of chemical reactions in the gas; $\nu''_{l,k}$ and $\nu'_{l,k}$ are the stoichiometric coefficients of the lth species in the mixture which is a product and reactant in the kth reaction, respectively; A is the preexponential factor; n is the temperature exponent; E is the activation energy; σ is the Stefan–Boltzmann constant; a_l and X_l are the emissivity and volume fraction of the lth emitting gas; α_s is the heat transfer coefficient between gas and PS; $S_{\text{PS}} = 6(1-\varphi)/d$ is the specific surface area of the PS (d is the characteristic size of solid skeleton in the PS); ε_s is the coefficient of radiation absorption by the PS material; δ_s is the delta function used to account for radiation absorption only on the PS surface; and μ is the dynamic viscosity of the gas. Equation (16) is used according to recommendations [11].

The values of parameters A, n, E, $\nu''_{l,k}$, $\nu'_{l,k}$, L, and N are taken from the detailed kinetic mechanism of fuel oxidation [12], supplemented by a semiempirical mechanism for the formation and oxidation of soot [13] based on three overall reactions with one additional component — soot C. In the mechanism [13], acetylene, which is present in the mechanism [12], is used as a soot precursor. The values of the parameters d_{soot} and ρ_{soot} are taken according to the recommendations [13]. The values of the coefficients a_l for H_2O and CO_2 are taken from the polynomials in [14]; for N_2 and O_2, a_l is independent of the gas temperature and is assumed to be equal to 0.1. The dynamic viscosity μ and thermal conductivity λ of the gas as well as the effective diffusion coefficients of species in the gas mixture, D_l, and specific heats $c_{p,l}$ are calculated by the formulae presented in [15].

Figure 2 shows the computational domain containing a planar 1D buffer channel, the PS, and the outer space. The planar 1D buffer channel with a length of $r_0 = 10$ mm is used to avoid distortion of the inlet boundary conditions in the PS. To avoid singularity in the PS center, a provision is made for the small internal cavity in the PS with the surface cross-section area equal to S_{in}.

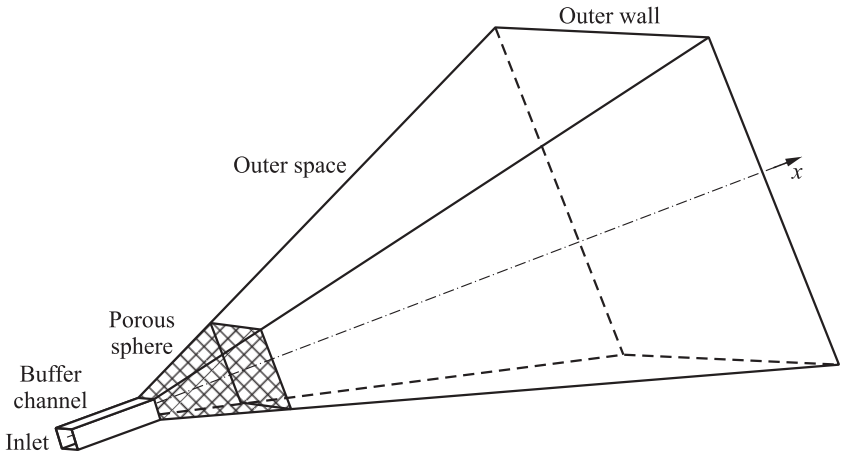

Figure 2 Computational domain

Initial conditions:

$$t = 0,$$

$$0 \leqslant x \leqslant r_\infty : \; P = P_0 \,; \; T = T_0 \,; \; T_s = T_0 \,; \; Y_l = \begin{cases} Y_{l0} \,, & l = \mathrm{O_2}, \mathrm{N_2} \,; \\ 0, & l \neq \mathrm{O_2}, \mathrm{N_2} \,. \end{cases}$$

Boundary conditions:

$$t > 0,$$

$$x = 0 : \quad \rho U S_{\mathrm{in}} = G_{\mathrm{in}} \,; \; T = T_0 \;\; ; \; Y_l = \begin{cases} Y_{l0}, & l = \mathrm{C_2H_4}, \mathrm{N_2} \,; \\ 0, & l \neq \mathrm{C_2H_4}, \mathrm{N_2} \,; \end{cases}$$

$$x = r_\infty : \qquad U = 0; \qquad T = T_0; \; \frac{\partial Y_l}{\partial x} = 0 \,, l = 1, \ldots, N \,.$$

The purpose of the calculations at this stage of research is to determine the spatial structure of the SDF and its evolution in time as well as the time histories of such characteristics of the SDP as the flame radius r_f, the temperature of the PS T_s, the maximum gas temperature (combustion temperature) $T_{g,\max}$, and the cumulated soot mass fraction $Y_{\mathrm{soot},\Sigma}$.

3.3 Numerical solution

The spherical part of the computational domain in Fig. 2 is represented by the spherical segment with a solid angle of 3°. The computational domain of Fig. 2 is

divided into 1333 control volumes compressed toward the external surface of the PS which was proved to ensure the grid independence of the calculation results. The set of 3D governing Eqs. (1) to (4) with additional relations (5) to (15) is solved by the control volume method using the segregated SIMPLE/PISO (semi-implicit method for pressure linked equation / pressure implicit split operator) algorithm. Convective transfer in the law of conservation of mass is approximated by the central difference and in the law of conservation of momentum by the TVD (total variation diminishing) scheme with the MINMOD limiter. For the finite-volume approximation of all other equations, the standard UPWIND scheme of the first order is used. Equation (4) is solved explicitly.

Before calculating the dynamics of SDF, a proper ignition procedure was developed. The main requirement to the ignition procedure was the weakest possible effect on the flow field caused by a localized pressure rise. Preliminary calculations showed that the stronger the ignition, the later the arising flow field becomes insensitive to it. The resulting procedure is as follows. In a time interval of 0.2–0.3 s after the start of fuel supply, in the region $x \in [r_s + \Delta_1, r_s + \Delta_2]$ ($\Delta_1 = 0.5$ mm and $\Delta_2 = 0.6$ mm), the mixture temperature is instantaneously changed to $T_{\text{ign}} = 1300$ K. These time interval and region are selected to allow for the formation of a small portion of flammable premixed fuel–oxidizer composition. The ignition temperature of 1300 K is found to be about the minimal temperature required for mixture ignition.

The following values of the governing parameters are used in the calculations: $T_0 = 293$ K, $P_0 = 0.1$ MPa (unless otherwise specified); $S_{\text{in}} = 5 \cdot 10^{-10}$ m^2; $r_s = 0.0032$ m; $r_\infty = 0.288$ m; $\varphi = 0.5$; $\kappa = 10^{-13}$ m^2; $d = 10^{-5}$ m; $\varepsilon_s = 0.8$; $\rho_s = 4000$ kg/m^3; $c_s = 650$ J/(kg·K); $\lambda_s = 5$ W/(m·K); $d_{\text{soot}} = 2$ nm; $\rho_{\text{soot}} = 2000$ kg/m^3; $N = 48$; and $L = 209$.

4 Results and Discussion

The table presents the baseline data for four selected experiments. The columns of the table from left to right show the flame number; mole fraction of ethylene in a combustible gas diluted with nitrogen (X_f); mole fraction of oxygen in the initial nitrogen–oxygen mixture (X_{O_2}); mass flow rate of ethylene through the PS (G_f); and the mass flow rate of the ethylene–nitrogen mixture through the

Conditions of experiments with SDFs

Flame	X_f	X_{O_2}	G_f, mg/s	G_{in}, mg/s	P_0, MPa
#2	0.29	0.40	0.52	1.80	0.100
#8	0.29	0.39	1.05	3.64	0.126
#10	1	0.38	1.24	1.24	0.127
#5	0.40	0.40	2.01	5.02	0.125

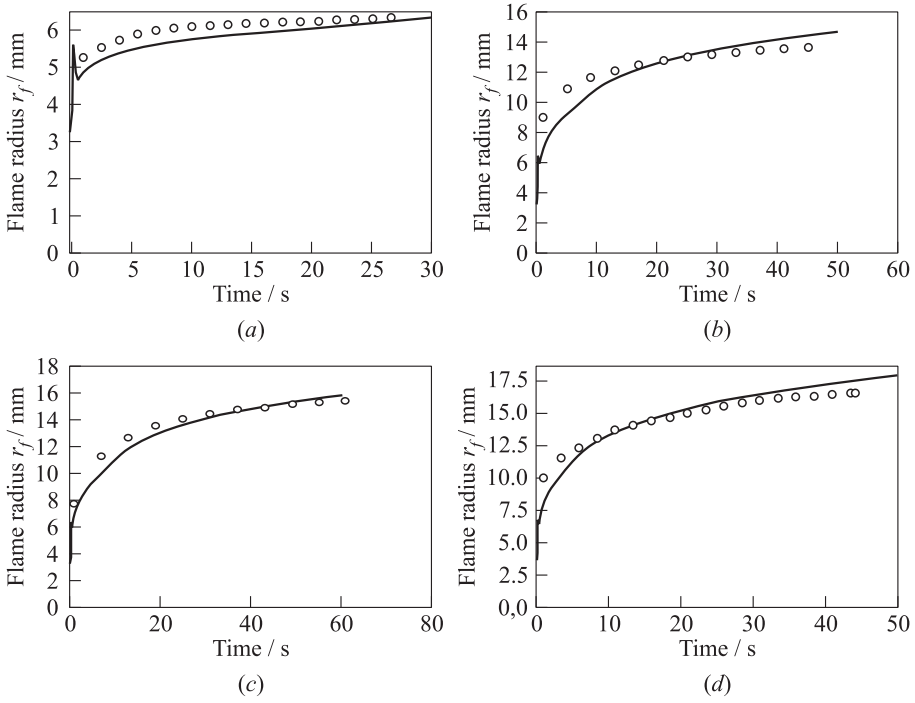

Figure 3 Comparison of predicted (curves) and measured (signs) time histories of flame radius: (*a*) flame #2; (*b*) #8; (*c*) #10; and (*d*) flame #5

PS (G_{in}) and the initial pressure in the CC (P_0). For all the flames, $X_{\text{O}_2} \approx 0.4$ and $P_0 \approx 0.1$ MPa.

Figure 3 compares the calculated time histories of the SDF radius with those measured in the experiments. In the calculations, the flame radius was determined as a coordinate of the maximum gas temperature, while in the experiments, it was determined from the size of the glow zone. Keeping in mind that the experimental error in measuring the flame radius this way could be significant, we note that the developed model satisfactorily describes the temporal evolution of the flame. There are some interesting observations in the data of Fig. 3. As seen, after ignition, all the flames move gradually outwards. At ~ 25 s after ignition (the shortest measurement time for the flames), flames #2 and #8 stay at ~ 6.5 and ~ 13 mm, respectively, from the center of the PS despite close values of X_f. The reason is apparently a twice higher mass flow rate G_{in} in flame #8. Interestingly, at ~ 25 s after ignition, flame #10 exhibits nearly the same standoff distance (~ 14 mm) as flame #8, despite its value of G_{in} is lower by a factor of nearly 3. The reason is seemingly the fact that the value of X_f for

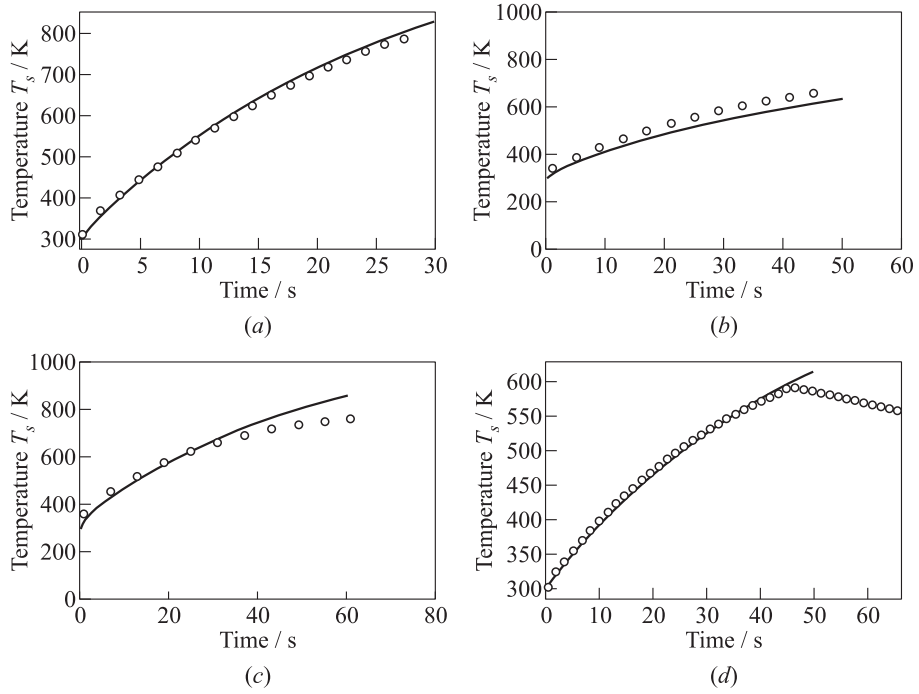

Figure 4 Comparison of predicted (curves) and measured (signa) time histories of PS temperature: (*a*) flame #2; (*b*) #8; (*a*) #10; and (*b*) flame #5

flame #10 is by a factor of 3 higher than for flame #8. This apparent consistency is, however, violated by flame #5. Thus, increase of X_f by about 40% (from 0.29 in flame #8 to 0.4 in flame #5) with the simultaneous increase in G_{in} by 40% (from 3.64 mg/s in flame #8 to 5.02 mg/s in flame #5) leads to the increase in the flame standoff distance only by 20% (from $\sim$ 13 mm for flame #8 to 15 mm for flame #5).

Figure 4 compares the calculated time histories of the PS temperature with those measured in the experiments. In the calculations, the temperature of the PS was determined as the average over the entire bulk of the PS (due to high thermal conductivity, the PS is heated up almost uniformly), while in the experiments, it was measured by a thermocouple, the junction of which was flush with the outer surface of the PS. The model is seen to describe satisfactorily the evolution of the PS temperature. Note that all the experiments under consideration were terminated because of a high value of PS temperature by cutting off the fuel supply. A closer location of flame #2 to the PS results in a fastest growth of the PS temperature among all the flames (see Fig. 4*a*). In the experiment of

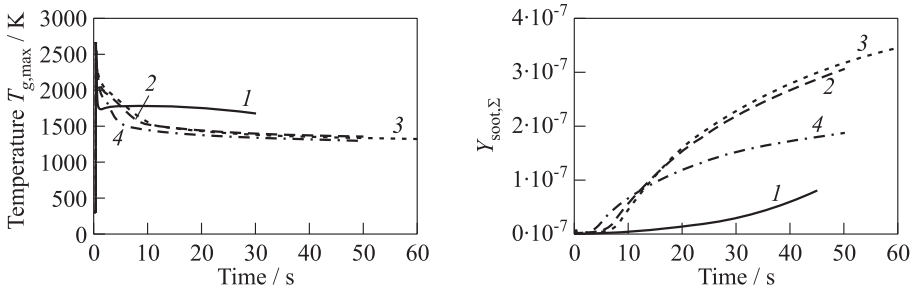

Figure 5 Predicted time histories of the maximum gas temperature (*a*) and cumulated soot mass fraction (*b*): *1* — flame #2; *2* — #8; *3* — #10; and *4* — flame #5

flame #5 (see Fig. 4*d*), the fuel supply was automatically turned off which is reflected by the kink on experimental points. Such situations were not modeled in the calculations.

Figure 5*a* shows the calculated time histories of the maximum gas temperature for the four SDFs presented in the table. Unfortunately, the gas temperature was not measured in these experiments. The model predicts a sharp temperature rise at ignition, which is followed by a transition period and the establishment of the quasi-steady diffusion combustion with the slowly decreasing maximum gas temperature for all the flames. The shortest transition period is inherent in flame #2 (about 1 s). The duration of the transition period for other flames is 5–10 s. The highest value of the maximum gas temperature during quasi-steady combustion is predicted for flame #2 (1700–1750 K), whereas flames #8, #10, and #5 exhibit the maximum gas temperature at a level of 1450–1500 K. The decrease in the maximum gas temperature is caused by the heat loss due to, mainly, the radiation of soot and triatomic molecules (CO_2 and H_2O).

Finally, Fig. 5*b* shows the calculated time histories of the cumulated soot mass fraction under conditions of all experiments in the table. The cumulated soot mass fraction is determined as the integral of soot mass fraction over the entire volume of the CC. The calculation shows the accumulation of soot in the CC, i. e., the flames under consideration are accompanied with soot formation. The overall amount of soot is quite low and differs from flame to flame. The minimum amount of soot accumulated in the CC is predicted for flame #2 with the highest maximum temperature. The largest amount of soot accumulated in the CC is predicted for flame #10 apparently because the fuel entering the PS is not diluted with nitrogen. To demonstrate the behavior of soot in the model, let us consider Figs. 6 and 7. Figure 6 shows the calculated structure of flame #10 20 s after ignition. The maximum concentration

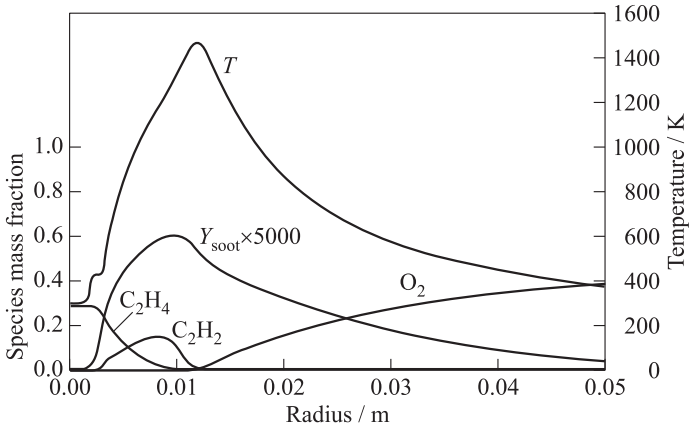

Figure 6 Spatial distributions of temperature and mass fractions of ethylene, oxygen, acetylene, and soot 20 s after ignition; sooting flame #10

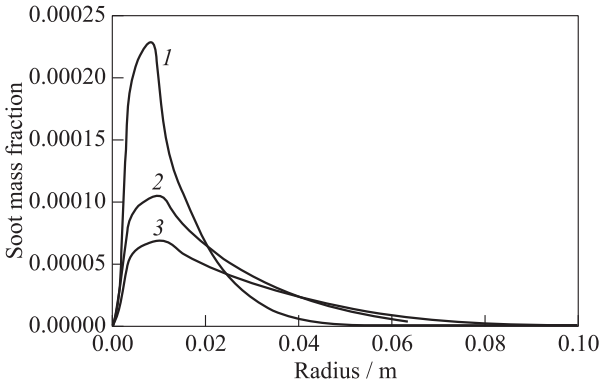

Figure 7 Spatial distributions of the soot mass fraction 10 (*1*), 20 (*2*), and 30 s (*3*) after ignition

of soot is reached in the flame itself (in the region of the maximum growth rate of acetylene concentration). Soot is seen to diffuse both towards the PS and outward (towards the outer wall of the CC). The latter is substantiated by the zero concentration of acetylene in this region. Due to the low temperatures, the soot formed in the flame is not virtually oxidized. Figure 7 shows the evolution of the calculated profile of the soot mass fraction in 10, 20, and 30 s after ignition. Despite a decrease in the maximum concentration of soot in the flame, soot is accumulated in the system which follows from the joint

consideration of Figs. 7 and 5*b* (curve *3*). Note that in the experiment, soot diffuses primarily towards the PS, whereas in calculations, soot diffuses both upstream (toward the PS) and downstream (through the flame). In the region downstream the flame, soot fails to oxidize due to low temperature and therefore accumulates. Such a behavior of soot in the calculations is probably explained by neglecting the thermodiffusion/thermophoresis phenomena in the model.

5 Concluding Remarks

Computer simulation is shown to reproduce the phenomenology of the spherical diffusion flame in microgravity conditions. This means that the underlying physical and mathematical model allows interpretation of the observed effects and even possesses some predictive power, at least qualitative. As a matter of fact, calculations satisfactorily predict the time histories of flame radius and PS temperature for the conditions when the mass flow rate of fuel mixture varies from 1 to 5 mg/s with the fuel content in the mixture ranging from 0.3 to 1. Calculations show the temporal decrease in the maximum flame temperature caused by the heat loss due to the radiation of soot and triatomic molecules (CO_2 and H_2O), which is consistent with observations indicating the gradual decay in flame brightness up to flame quenching. Also, despite the simplified modeling of soot formation, calculations show that soot forms in the fuel-rich region slightly upstream of the temperature peak. The amount of soot formed depends on experimental conditions and increases with the fuel concentration in the gas entering the PS. However, contrary to observations with soot diffusing primarily towards the PS, in calculations soot diffuses both upstream (towards the PS) and downstream (through the flame). In the region downstream from the flame, soot fails to oxidize due to low temperature and therefore accumulates. Such a behavior of soot in the calculations is probably explained by neglecting the thermodiffusion/thermophoresis phenomena in the model. Further studies will be focused on resolving this issue and on the flame quenching phenomenon.

Acknowledgments

This work is implemented within the spacecraft experiment “Adamant.” The author is grateful to his colleagues at the N. N. Semenov Federal Research Center for Chemical Physics of the Russian Academy of Sciences (V. Ya. Basevich, A. A. Belyaev, F. S. Frolov, S. N. Medvedev, V. S. Posvyanskii, M. Yu. Sinev, and P. A. Vlasov) as well as to R. L. Axelbaum of Washington University in St. Louis, P. B. Sunderland of the University of Maryland, and D. L. Urban of the NASA Glenn Research Center for fruitful collaboration.

References

1. Flickr. Available at: www.flickr.com/photos/space-flames (accessed March 26, 2021).
2. Space Flames. Available at: www.facebook.com/space.flames (accessed March 26, 2021).
3. Zarevo. Available at: https://tsniimash.ru/science/scientific-experiments-onboard-the-is-rs/cnts/experiments/zarevo/ (accessed March 26, 2021).
4. Sunderland, P. B., R. L. Axelbaum, D. L. Urban, B. H. Chao, and S. Liu. 2003. Effects of structure and hydrodynamics on the sooting behavior of spherical microgravity diffusion flames. *Combust. Flame* 132:25–33.
5. Christiansen, E. W., S. D. Tse, and C. K. Law. 2003. A computational study of oscillatory extinction of spherical diffusion flames. *Combust. Flame* 134:327–337.
6. Tang, S., M. K. Chernovsky, H. G. Im, and A. Atreya. 2010. A computational study of spherical diffusion flames in microgravity with gas radiation Part I: Model development and validation. *Combust. Flame* 157:118–126. doi: 10.1016/j.combustflame.2009.09.010.
7. Lecoustre, V. R., P. B. Sunderland, B. H. Chao, and R. L. Axelbaum. 2012. Numerical investigation of spherical diffusion flames at their sooting limits. *Combust. Flame* 159:194–199. doi: 10.1016/j.combustflame.2011.05.022
8. Nayagam, V., D. L. Dietrich, and F. A. Williams. 2019. Radiative extinction of burner-supported spherical diffusion flames: A scaling analysis. *Combust. Flame* 205:368–370. doi: 10.1016/j.combustflame.2019.04.027.
9. Markan, A., H. R. Baum, P. B. Sunderland, J. G. Quintiere, and J. L. de Ris. 2020. Transient ellipsoidal combustion model for a porous burner in microgravity. *Combust. Flame* 212:93–106. doi: 10.1016/j.combustflame.2019.09.030.
10. Williams, F. A. 1985. *Combustion theory*. Menlo Park, CA: The Benjamin/Cummings Publishing Co., Inc. 636, 637.
11. Forchheimer, P. 1901. Wasserbewegung durch boden. *Z. Ver. Dtsch. Ing.* 45(50):1781–1788.
12. Basevich, V. Ya., A. A. Belyaev, V. S. Posvyanskii, and S. M. Frolov. 2013. Mechanisms of the oxidation and combustion of normal paraffin hydrocarbons: Transition from C_1–C_{10} to C_{11}–C_{16}. *Russ. J. Phys. Chem. B* 7(2):161–169. doi: 10.1134/S1990793113020103.
13. Basevich, V. Ya., S. N. Medvedev, S. M. Frolov, F. S. Frolov, B. Basara, and P. Prieching. 2016. Makrokinetitcheskaya model' dlya rastcheta emissii sazhi v dizele [Macrokinetic model for calculating soot emission in Diesel engine. *Goren. Vzryv (Mosk.) — Combustion and Explosion* 9(3):36–46.
14. TNF Workshop. Availbale at: https://tnfworkshop.org/radiation/ (accessed March 26, 2021).
15. Reid, R. C., J. M. Prausnitz, and T. K. Sherwood. 1977. *The properties of gases and liquids*. 3rd ed. McGraw-Hill chemical engineering ser. New York, NY: McGraw-Hill. 703 p.

СФЕРИЧЕСКОЕ ДИФФУЗИОННОЕ ПЛАМЯ В УСЛОВИЯХ МИКРОГРАВИТАЦИИ: ПЕРВЫЕ РЕЗУЛЬТАТЫ СОВМЕСТНОГО РОССИЙСКО-АМЕРИКАНСКОГО КОСМИЧЕСКОГО ЭКСПЕРИМЕНТА FLAME DESIGN (АДАМАНТ)

С. М. Фролов

Федеральный исследовательский центр химической физики
им. Н. Н. Семёнова Российской академии наук (ФИЦ ХФ РАН)
Россия, Москва 119991, ул. Косыгина, д. 4

Совместный космический эксперимент (КЭ) НАСА и Роскосмоса Flame Design (Адамант) — один из шести экспериментов, проводимых в настоящее время астронавтами НАСА и космонавтами Роскосмоса на Американском сегменте Международной космической станции в рамках проекта ACME (русский перевод: «Продвинуться в понимании горения с помощью экспериментов в условиях микрогравитации»). Исходный план эксперимента разработан американскими коллегами — профессорами Р. Аксельбаумом из Вашингтонского университете в Сэнт-Луисе и П. Сандерлэндом из Университета шт. Мэрилэнд, а также д-ром Д. Урбаном из Исследовательского центра Гленн НАСА. Задача российских ученых из ФИЦ ХФ РАН в этом проекте (С. М. Фролов, В. Я. Басевич, А. А. Беляев, Ф. С. Фролов, С. Н. Медведев, В. С. Посвянский, М. Ю. Синев, П. А. Власов) — вместе с американскими коллегами участвовать в сопровождении и дальнейшем планировании эксперимента по ходу получения и обработки результатов.

Цель КЭ — экспериментальное и теоретическое изучение фундаментальных механизмов управления сажеобразованием в сферическом диффузионном пламени (СДП), формируемом вокруг пористой сферы, и радиационного погасания СДП в условиях микрогравитации. Объекты исследования — «прямые» и «обратные» СДП газообразного этилена в атмосфере кислорода с добавками инертных газов, азота и диоксида углерода при давлениях от 0,2 до 1 атм и при комнатной температуре. «Прямое» пламя — это пламя, образованное в атмосфере окислителя при подаче горючего через пористую сферу. «Обратное» пламя — это пламя, образованное в атмосфере горючего при подаче окислителя через пористую сферу. Данные КЭ используются для проверки одномерных, двумерных и трехмерных физико-матема-

тических моделей явления, включающих сокращенные и детальные кинетические механизмы окисления и горения этилена, сажеобразования, свойства переноса в многокомпонентной газовой смеси, а также конвективный и кондуктивный теплообмен и теплообмен излучением. Ожидается, что в результате выполнения проекта будут получены новые знания о физике и химии диффузионных пламен, которые помогут в решении задач управления горением и снижения вредных выбросов при горении. Представлены текущие экспериментальные и теоретические результаты проекта.

Работа выполнена в рамках КЭ «Адамант».